





Techniques for the generation of multiple additional transmission zeros in H-plane waveguide filters

Daniel Miek , Patrick Boe , Fynn Kamrath  and Michael Höft 

Kiel University, Kiel, Germany

Research Paper

Cite this article: Miek D, Boe P, Kamrath F, Höft M (2020). Techniques for the generation of multiple additional transmission zeros in H-plane waveguide filters. *International Journal of Microwave and Wireless Technologies* **12**, 723–732. <https://doi.org/10.1017/S1759078720000811>

Received: 8 November 2019

Revised: 20 May 2020

Accepted: 21 May 2020

First published online: 24 June 2020

Key words:

Additional transmission zeros; frequency-dependent coupling aperture; Ku-band waveguide filter; resonant transmission zeros (TZs)

Author for correspondence:

Daniel Miek, E-mail: dami@tf.uni-kiel.de

Abstract

In this paper, different techniques for the generation of additional transmission zeros (TZs) in planar waveguide filters are investigated. In the classical theory, TZs are generated only by destructive interference of non-adjacent cavities, limiting the available number of TZs to the filter order itself. However, more approaches for the generation of TZs are known, including bypass-coupling in oversized cavities, frequency-dependent coupling apertures as well as dispersive/resonant TZs which can be realized by the direct source to load cross-coupling. The aim of this paper is to combine several of the strategies in one physical filter set-up to increase the maximal number of TZs beyond the filter order. Different Ku-band fourth-order filter set-ups are presented, showing in total between six and eight real as well as complex TZs. Three filters are manufactured as a proof of concept and compared with the simulation, showing very good agreement.

Introduction

Due to the high number of mobile and satellite communication services, the electro-magnetic spectrum is getting more crowded and the resource “bandwidth” is becoming scarce. The performance of the filters especially at the output stage after amplification is very important to fulfill the stringent out-of-band rejection requirements of a transmitter system. Depending on the application of the filter to be designed, requirements in terms of near-band rejection, losses, and volume/weight are often in the focus of interest.

Transmission zeros (TZs) are important in the filter design process as the near-band selectivity of the filter can drastically be improved without increasing the filter order n and hence the associated losses [1]. Real- and complex TZs might be realized by destructive and constructive interference, respectively. The importance of complex pairs of TZs is mainly defined by the phase linearity constraints.

Nevertheless, the classical approach as comprehensive presented in e.g. [1] has fundamental limitations. TZs might only be realized by cross-couplings or extracted pole sections. The first type may lead to difficult to realize diagonal cross-couplings, which is often a severe problem especially in waveguide filters. Extracted pole filters are an interesting alternative but suffer from an increased footprint due to the need of non-resonating nodes which couple the extracted pole resonators [2]. A further limitation is the theoretical maximal number of TZs n_{fz} which is limited by the filter order n itself and cannot exceed it.

These limitations are circumvented in the set-ups presented in this paper. Different techniques for the generation of TZs are combined within one filter set-up, leading to in total up to eight real frequency axis TZs by a filter order of $n = 4$. Apart from classical destructive interference, bypass-couplings as proposed in e.g. [3, 4] are used to increase the total number of TZs. Additionally, a frequency-dependent coupling aperture [5–8] is able to introduce one additional TZ by replacing a classical (non-resonant) coupling aperture. Furthermore, the direct source to load (SL) coupling is able to realize two types of TZs simultaneously. On the one hand, TZs are generated by the classical destructive interference while on the other hand dispersive/resonant TZs might additionally occur [9–12].

Four slightly different filter set-ups are presented in this paper which make use of some of the TZ generating mechanism or even all. This paper is organized as follows. Based on [13], the basic filter set-up is shortly repeated in section “Basic filter set-up”. In section “Phase equalized filter with six TZs”, it is shown that the proposed set-up is able to realize a complex pair of TZs for phase equalization as well, leading to in total six TZs. The total number of TZs might be increased by using a double-slotted source to load cross-coupling aperture as described in section “Filter set-up with double source to load coupling” while section “Filter set-up with additional frequency-dependent coupling structures” exploits the use of frequency-dependent coupling apertures. Section “Conclusion” concludes this paper.

Basic filter set-up

The basic filter set-up was first proposed in [13] and is repeated in Fig. 1 for the sake of clarity. The desired filter specifications are set to the lower and upper passband edge of $f_1 = 14$ GHz

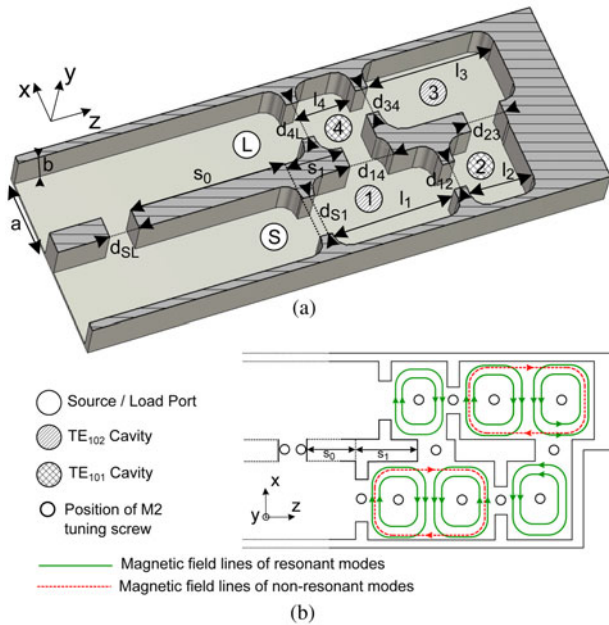


Fig. 1. Basic filter set-up for the realization of up to seven real frequency axis TZs. Dimensions are identical as proposed in [13]. The dimensions of the waveguide are chosen according to the Ku-band standard: $a = 15.7988$ mm and $b = 7.8994$ mm.

and $f_2 = 14.25$ GHz, respectively, while the desired return-loss in the passband is set to $RL = 20$ dB. Two TZs in the initial design are foreseen at normalized frequency $f_{TZ,Lp} = \pm j2$. The associated coupling topology is a quadruplet with a negative coupling factor between cavity one and four (m_{14}) [14]. The synthesis of the ini-

magnetic couplings might easily be realized through the bottom/cover of a cavity. Depending on the position of the coupling aperture (e.g. near the side wall or in the center), the magnetic or even electric field coupling dominates [9, 10]. For lower frequencies, even small probes for the coupling of electric fields are possible [17]. Nevertheless, in higher frequency ranges, aperture couplings are preferred, as the tuning of e.g. probes becomes complicated and the losses increase. The solution used here for the realization of a negative coupling factor m_{14} is to turn around the direction of the magnetic fields in oversized cavities as e.g. proposed in [18]. Therefore, cavity two and four are designed to resonate at their basic TE_{101} mode whereas cavity one and three resonate at the TE_{102} mode. Figure 1(b) gives an overview over the relative positions of the cavities as well as the magnetic fields at center frequency. Note that the magnetic fields in adjacent cavities along the main-line are oppositely oriented to each other. The coupling factor of two adjacent cavities i and j is proportional to the electric and magnetic fields, which couple through the aperture according to (1).

$$k_{ij} \propto -H_i \cdot H_j + E_i \cdot E_j \quad (1)$$

By comparing the direction of the magnetic fields with the definition in (1), all main-line couplings realize a positive coupling factor. However, considering the cross-coupling aperture, it becomes obvious that a negative coupling factor between cavity one and four arises. The electric field component in (1) can be neglected in this case as there are only magnetic coupling apertures. Therefore, two TZs are generated by the destructive interference between cavity one and four.

	S	1	2	3	4	5	6	7	L
S	0.0	2.4314	-0.1828	0.0	-0.0033	0.0254	-0.0313	0.4900	0.0042
1	2.4314	0.4346	1.3167	0.0	-0.1674	0.0044	-0.0047	-1.4135	0.0
2	-0.1828	1.3167	0.0283	0.5156	-0.6704	0.0	0.0	0.0	0.0
3	0.0	0.0	0.5156	0.4865	1.2595	0.0	0.0	0.0	0.0
4	-0.0033	-0.1674	-0.6704	1.2595	0.5799	4.0017	-4.1170	-0.2794	2.1851
5	0.0254	0.0044	0.0	0.0	4.0017	-3.0413	-0.7706	0.0	-0.0079
6	-0.0313	-0.0047	0.0	0.0	-4.1170	-0.7706	4.2483	0.0419	-0.3448
7	0.4900	-1.4135	0.0	0.0	-0.2794	0.0	0.0419	-1.4715	-0.0023
L	0.0042	0.0	0.0	0.0	2.1851	-0.0079	-0.3448	-0.0023	0.0

tial filter dimensions is accomplished based on [1, 15]. First, sub-structures (two cavities coupled by a blend aperture) are simulated to find the correct coupling factors in terms of eigenmode simulations. The length of the different cavities can be estimated by the loading as described in [1] Ch. 14.5. Finally, the fine tuning of the filter takes place by coupling matrix extraction and adjustment techniques using the Cauchy method [16]. Note that the filter dimensions obtained here are used as a basis for the further adaptations made in the next sections.

For the realization of the two real frequency axis TZs, a negative cross-coupling between resonator one and four is required [13]. Many approaches are known in the literature for the realization of negative coupling factors in waveguide filter techniques. Stacked filter topologies are a common solution as electric and

However, as discussed in [13], additional coupling paths between the source port and cavity two (m_{s2}), the source port and cavity four (m_{s4}) as well as cavity two and four (m_{24}) arise. The reason is that the basic TE_{10} mode is excited in the oversized cavities one and three, realizing bypass couplings for the generation of an additional TZ above the passband of the filter. The corresponding field lines of the basic non-resonant modes are shown in Fig. 1(b) while the associated coupling scheme is shown in Fig. 2(a). A modeling of the bypass couplings with non-resonant nodes in the coupling scheme would be possible as well, but as discussed in [3] the design by using “classical” coupling paths is sufficient in the considered case.

The filter of Fig. 1(a) was manufactured as a proof of concept in brass as a conventional H-plane filter. Tuning screws can be

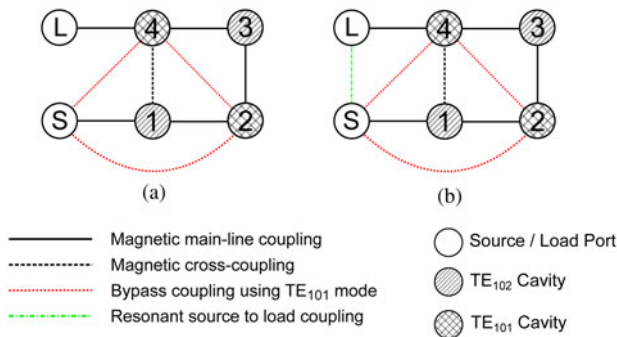


Fig. 2. Coupling schemes of the filter set-up from Fig. 1: (a) set-up without direct source to load cross-coupling and (b) set-up with direct source to load cross-coupling [13].

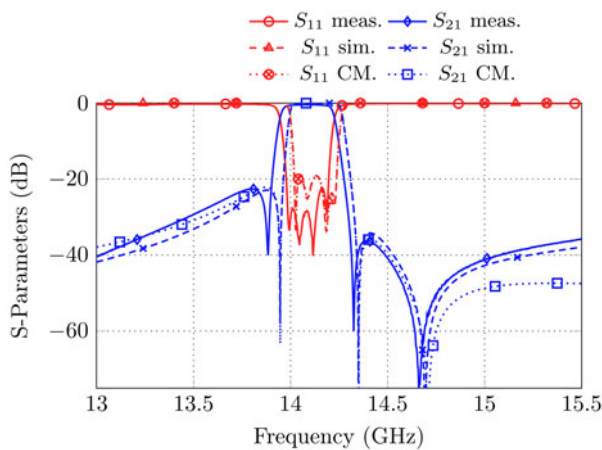


Fig. 3. Measured S-parameters in comparison to simulation and the coupling matrix from Table 1. The outer TZ at 14.7 GHz arises by bypassing the oversized cavities [13].

inserted in the cover of the filter at positions indicated by circles in Fig. 1(b). The measurement results in comparison to the simulation are shown in Fig. 3. Three TZs as expected by the simulation and the coupling diagram of Fig. 2(a) arise while a quality factor of $Q_u \approx 2100$ can be reached. Please note that until now the direct source to load cross-coupling as shown in Fig. 1(a) is not used and was therefore closed by a small brick for the measurement.

A suitable coupling matrix for the topology in Fig. 2(a) might be calculated by a series of similarity transformations, starting from the filter polynomials calculated by e.g. [19]. An alternative to similarity transformations is the calculation of coupling matrices by optimization as basically proposed in [20]. The coupling matrix which fits the simulation results over nearly the whole frequency

range is given in Table 1 and was found by optimization. The coupling matrix proposed in [13] was used as a starting point for the optimization and the additional coupling factors m_{S2} , m_{S4} as well as m_{24} are enabled as additional variables to account for the bypass couplings. The S-parameters of the coupling matrix are plotted in Fig. 3 as well. As can be seen, only small deviations far away from the passband arise while the position of the TZs are in good accordance. The bypass couplings can be modeled as simple coupling paths between the corresponding resonators with relatively small coupling-strengths due to the inferior excitation [3].

Additional TZs might be realized by including the direct source to load cross-coupling as implied by Fig. 1. This cross-coupling is able to introduce more than the two expected TZs by exploiting standing waves in the source/load port. For this reason, it might be necessary to shift this aperture relatively far away from the actual filter structure, which may be problematic in low-frequency ranges. However, the filters proposed here can be down scaled to higher frequencies where the focus is often not on size constraints while manufacturing tolerances are an issue. The fabrication of a coupling slot between the source and the load port might be easily realizable as the manufacturing of several cavities, which fulfill similar attenuation requirements in the stopband.

In [13], parameter studies in terms of the distance of the source to load coupling aperture s_0 as well as the diameter d_{SL} were accomplished, realizing the simplified coupling scheme in Fig. 2(b). Depending on the position of the SL coupling aperture in relation to the position of the input/output coupling blend, multiple TZs may occur [12].

In e.g. [9, 10], two additional TZs (in total four TZs) were generated by introducing an SL coupling in a symmetrical filter set-up. Depending on parameters s_0 and d_{SL} , four TZs are introduced by the source to load coupling in this set-up as well. A measurement result for parameters $s_0 = 31.8$ mm and $d_{SL} = 5.6$ mm is shown in Fig. 4(a). Other meaningful parameter combinations are possible as well [13]. The Q-factor remains unchanged compared to the first measurement while now a high suppression above the passband is realized by four successive TZs.

It is furthermore possible to find a coupling matrix description even for the improved design based on the coupling diagram proposed in [12]. There, a source-load cross-coupled fourth-order dual-band filter with two extra TZs is investigated (in total six TZs arise). The extra TZs are modeled by two additional de-tuned resonators in the source/load port. In total, six resonators are necessary to model the near passband behavior and the six TZs correctly. A very similar approach with six resonators is used in the following section “Phase equalized filter with six TZs” to determine the coupling matrix of a fourth-order phase equalized filter with in total six TZs as well.

$$\begin{matrix} & S & 1 & 2 & 3 & 4 & 5 & 6 & L \\ \begin{matrix} S \\ 1 \\ 2 \\ 3 \\ 4 \\ 5 \\ 6 \\ L \end{matrix} & \begin{pmatrix} 0.0 & 1.6366 & 0.1455 & 0.0 & -0.0321 & 1.4732 & 0.0 & -0.0375 \\ 1.6366 & -0.9014 & 1.0662 & 0.0 & 0.5244 & -3.2741 & 0.0 & 0.0 \\ 0.1455 & 1.0662 & 0.1558 & 0.5551 & -0.1040 & 0.0 & 0.0 & 0.0 \\ 0.0 & 0.0 & 0.5551 & 0.1338 & 1.0549 & 0.0 & 0.0 & 0.0 \\ -0.0321 & 0.5244 & -0.1041 & 1.0549 & -0.9762 & 0.0 & 1.4089 & 1.9839 \\ 1.4732 & -3.2741 & 0.0 & 0.0 & 0.0 & -11.1744 & -0.3179 & 0.0 \\ 0.0 & 0.0 & 0.0 & 0.0 & 1.4089 & -0.3179 & 7.6060 & 2.4624 \\ -0.0375 & 0.0 & 0.0 & 0.0 & 1.9839 & 0.0 & 2.4624 & 0.0 \end{pmatrix} & \end{matrix} \quad (3)$$

Table 1. Coupling matrix of the topology in Fig. 2(a) to fit the simulated S-parameters in Fig. 3

	S	1	2	3	4	L
S	0.0	0.939	-0.064	0.0	-0.041	0.0
1	0.939	0.02	0.75	0.0	-0.2	0.0
2	-0.064	0.75	0.008	0.679	0.083	0.0
3	0.0	0.0	0.679	-0.21	0.779	0.0
4	-0.041	-0.2	0.083	0.779	-0.05	0.998
L	0.0	0.0	0.0	0.0	0.998	0.0

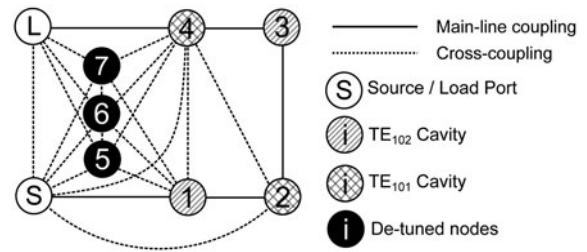


Fig. 5. Coupling diagram to fit the simulated S-parameters in Fig. 4 based on the description in [12].

$$S_{21}(s) = \frac{P(s)/\epsilon}{E(s)} \tag{5}$$

where $E(s)$ and $F(s)$ are of degree n and $P(s)$ is of degree n_{fz} . The order of $P(s)$ determines the number of TZs. However, as a filter is a passive system, the condition $n \geq n_{fz}$ must be fulfilled. It is therefore required to add $n_{fz} - n$ de-tuned nodes to the coupling scheme. The proposed topology is shown in Fig. 5 with the corresponding coupling matrix in (2), which was found by optimization. As a starting point, the entries of the coupling matrix in Table 1 were used and all entries according to the coupling scheme in Fig. 5 are enabled for optimization. It is possible to fit the simulated S-parameter response over nearly the whole simulation range as shown in Fig. 4(b), where the simulation results are compared with the S-parameters generated from the coupling matrix. However, multiple couplings between the de-tuned resonators and the remaining nodes are necessary for a sufficient coupling matrix fit wherefore the physical clarity suffers. In the following section “Phase equalized filter with six TZs”, a more suitable coupling matrix and topology for a six TZ filter is proposed.

Phase equalized filter with six TZs

The filter set-up proposed in section “Basic filter set-up” (Fig. 1) can be used in different configurations. By changing the parameter s_1 , which defines the position of the cross-coupling aperture between cavity one and four on the z -axis, a phase equalized filter might be realized by exploiting a complex pair of TZs. For relatively large values of s_1 , it is obvious that destructive interference arises between the right magnetic circle of cavity one and the magnetic field in cavity four (compare Fig. 1(b)), realizing two real frequency axis TZs as proven by the measurements in Fig. 3. However, for small values of s_1 , constructive interference between cavity one and four arises. In this case, the left magnetic circle in cavity one couples with the magnetic field in cavity four, implementing a coupling with equal sign as the main-line couplings. The filter of section “Basic filter set-up” was used as a starting point and the Trust Region Framework in CST Microwave Studio as well as coupling matrix extraction techniques are used to adapt the filter dimensions. Simulation results for a filter set-up without a direct source to load coupling show in total three TZs, two of which realize a complex pair while the real frequency axis TZ arises below the passband. However, for the direct source to load coupled filter set-up, a maximal number of six TZs can be reached. The simulated S-parameter response is shown in Fig. 6(a).

The presence of a complex pair of TZs is proven by the relatively flat group delay compared to the filter with seven real

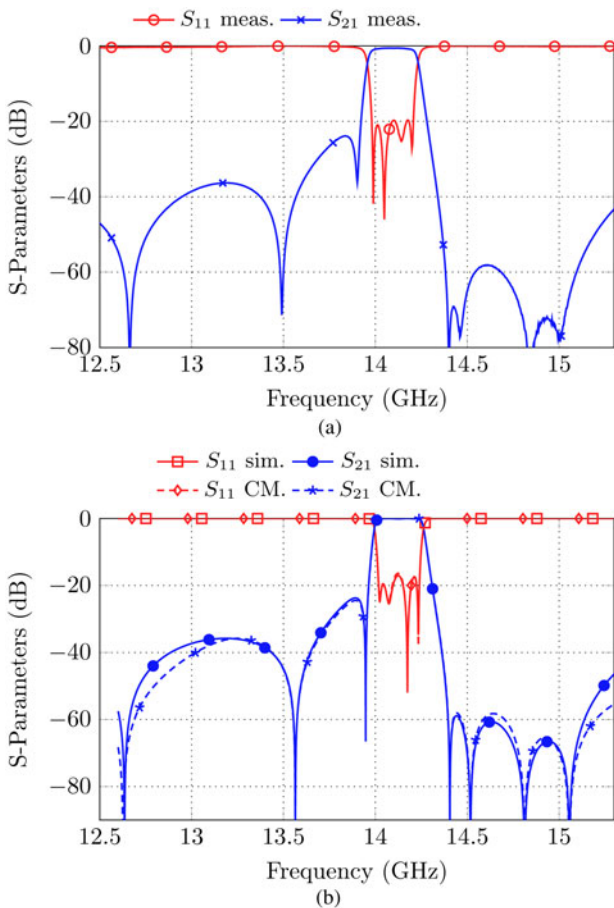


Fig. 4. (a) Measurement results of the filter set-up shown in Fig. 1(a) with additional source to load cross-coupling (with parameters $s_0 = 31.8$ and $d_{SL} = 5.6$) [13], (b) comparison of the simulated S-parameters with the coupling matrix in (2).

Nevertheless, in the case investigated here in total seven instead of six TZs are observed, therefore one more, i.e. three, de-tuned resonators are assumed between the source/load port based on the approach in [12]. Please note that in the case investigated here the number of TZs determines the number of nodes in the coupling matrix. $n = 4$ nodes are resonant while $n_{fz} - n = 3$ nodes must be de-tuned. The reason can be found in the description of the S-parameters according to [1]:

$$S_{11}(s) = \frac{F(s)/\epsilon_r}{E(s)} \tag{4}$$

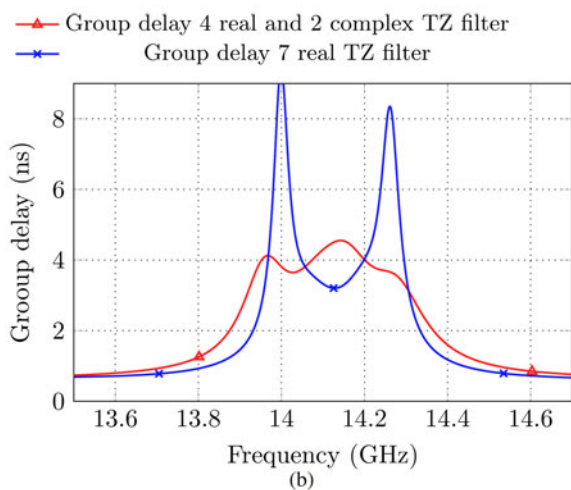
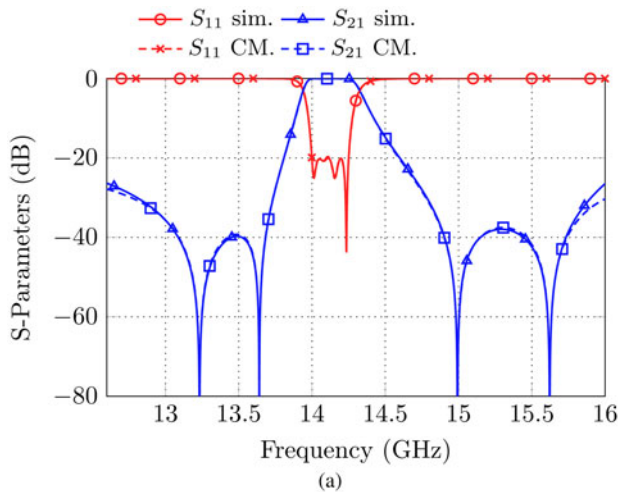


Fig. 6. (a) Simulated S-parameters in comparison to the S-parameters from the coupling matrix in (3) for the phase equalized fourth-order filter. (b) Comparison of the group-delay of the phase equalized filter and the 7 TZ filter from section “Basic filter set-up”.

frequency axis TZs, as shown in Fig. 6(b). The group delay variation within the passband is limited to less than 1 ns. The filter with seven real TZs shows a variation of roughly 5 ns from the passband center to the edge of the passband. The S-parameters of Fig. 6(a) are found for parameters $s_0 = 5$ mm, $d_{SL} = 8.25$ mm, and $s_1 = 8$ mm. In the considered case, the physical source to load cross-coupling aperture is quite close to the cavities, which does not influence the footprint significantly.

A coupling matrix which fits the simulated S-parameter response might be found by adding two further de-tuned resonators close to the source/load port, similar to the approach in section “Basic filter set-up” [12]. These resonators account for the distance between the source and load port to the cross-coupling and are necessary to model the additional TZs. The coupling matrix to fit the adapted topology in Fig. 7 is shown in (3). A comparison of the S-parameters from simulation and the response from the coupling matrix is shown in Fig. 6(a) and shows very good agreement. The coupling matrix is again found by optimization, where the coupling matrix in Table 1 is used as a starting point. The resonators five and six are strongly de-tuned, which becomes obvious by observing the main-diagonal in (3). Nevertheless, this coupling matrix has a better

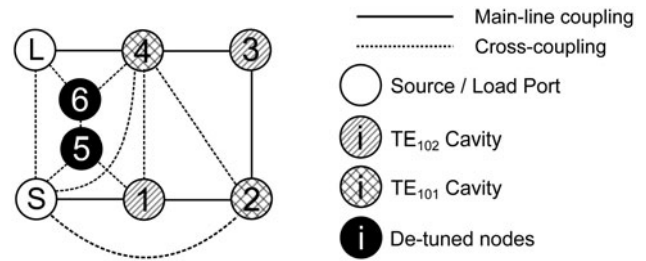


Fig. 7. Coupling topology for the coupling matrix in (3).

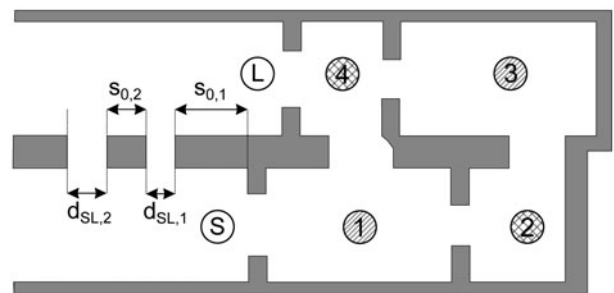


Fig. 8. Schematic view of the proposed filter set-up with a double-slotted source to load coupling.

physical clarity as there are less couplings necessary between resonator five/six and source/load or resonator one/two compared to the coupling matrix in (2).

Filter set-up with double source to load coupling

The aim of this section and the following one is to increase the total number of TZs provided by the filter set-up within the useful frequency region of the Ku-band. Two approaches are therefore investigated: in this section, the influence of a double-slotted source to load coupling on the number of TZs is examined, while in section “Filter set-up with additional frequency-dependent coupling structures”, additional frequency-dependent coupling structures are added to the physical filter set-up.

The basic filter structure investigated in this section is similar to the one proposed in Fig. 1(a) and is shown in Fig. 8 for the sake of clarity. Identical filter specifications are desired for an easy comparability among the set-ups. The additional TZs in section “Basic filter set-up” are mainly realized by the dispersive/resonant behavior of the source to load cross-coupling. Far away from the passband of the filter, standing waves arise due to the reflected energy from the first blend in the source/load port. These standing waves interfere constructively or destructively with each other, depending on the frequency as well as on the position and diameter of the source to load coupling. An empirical approach is therefore to add a further slot in the parallel source/load port for the realization of a double-slotted source to load coupling. The basic structure with parameters $s_{0,1} = 34.224$ mm, $s_{0,2} = 6.693$ mm, $d_{SL,1} = 4.1$ mm, and $d_{SL,2} = 5.5$ mm is shown in Fig. 8, while Fig. 9 shows a photo of the manufactured filter. To increase the Q-factor, the lower half as well as the cover were manufactured in aluminium. Tuning screws can be inserted at identical positions as in Fig. 1(b).



Fig. 9. Manufactured filter with a double-slotted source to load coupling.

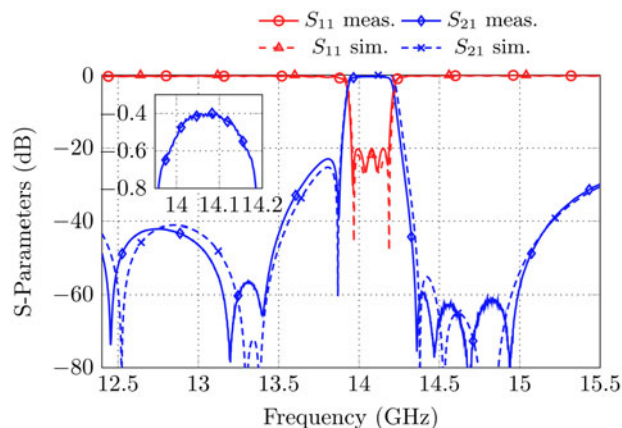


Fig. 10. S-parameter response of the manufactured filter from Fig. 9 in comparison to the simulation.

As can be seen in the measurement results in Fig. 10, in total eight TZs in the usable frequency region of the Ku-band can be realized. Above the passband, the appearance of the TZs is similar to the one in Fig. 4. Nevertheless, below the passband, four TZs are now generated as well. Compared to former measurements, the attenuation behavior above the passband is nearly identical but below the passband an improvement can be noticed. All in all, the measurement results show good agreement with the simulation and the position of all TZs is nearly as expected. The inset in Fig. 10 shows the insertion loss performance in the passband, which corresponds to a $Q_u \approx 2700$.

Filter set-up with additional frequency-dependent coupling structures

Filter set-up without source to load cross-coupling

The aim of the following investigation is to increase the number of available TZs of the basic Ku-band filter set-up from section “Basic filter set-up” by using frequency-dependent coupling structures. Different types of frequency-dependent couplings were investigated in the literature until now, e.g. [5–8, 21, 22]. The advantage of these structures is that TZs might be realized in an in-line configuration without requiring cross-couplings between non-adjacent cavities or extracted pole cavities. A commonly known structure of a frequency-dependent coupling aperture is a partial height post, as proposed the first time in [22] for the application in band-stop filters. The utilization in in-line band-pass filter configurations was proven in [7, 21] while in [5] the application within a cross-coupling was proposed to

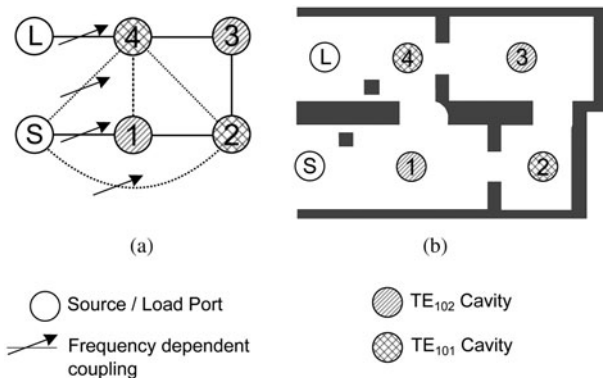


Fig. 11. (a) Topology of the fourth-order Ku-band filter with frequency-dependent couplings between the source port and cavity one as well as cavity four and the load port and (b) position of the frequency-dependent posts in the overall filter set-up.

increase the number of TZs generated by a quadruplet from two to three. However, the combination of frequency-dependent coupling structures with usual cross-couplings, bypass couplings as well as a direct source to load coupling was not investigated until now to the best of the authors knowledge.

The basic filter structure is similar to the one proposed in section “Basic filter set-up” (Fig. 1), where now the former inductive couplings between the source port and cavity one as well as cavity four and the load port are replaced by a partial height post, leading to the coupling diagram in Fig. 11(a) and the filter structure in (b). All couplings which are now realized by a frequency-dependent coupling are marked by an arrow. Please note that also the bypass couplings m_{S2} and m_{S4} become frequency-dependent by the insertion of a partial height post in the source port. Furthermore, the topology in Fig. 11(a) needs no additional de-tuned resonators as at this point the filter is investigated without a direct source to load cross-coupling. The presence of additional TZs can be modeled by the frequency-dependent couplings generated by the partial height posts.

The basic structure of a post within a waveguide channel with all available degrees of freedom is shown in Fig. 12(a). The discrete equivalent circuit is shown in Fig. 12(b) and is identical to the one proposed in [23], where the partial height post was investigated in depth. A classical T -inverter is assumed where the series impedances $Z_1 + Z_2$ load the adjacent resonators. The frequency dependence of the coupling factor K can be calculated directly from the S-parameters, which are obtained by EM-simulations. Relation (6) can be obtained by equating the $ABCD$ parameters of an ideal inverter with the ones generated by the equivalent circuit from Fig. 12(b).

$$\frac{K}{Z_0} = \text{Im} \left(\frac{2 \cdot S_{21}}{(1 - S_{11}) \cdot (1 - S_{22}) - S_{12} \cdot S_{21}} \right) \quad (6)$$

Note that a phase de-embedding of the S-parameters to the center of the post is necessary for the evaluation of the equation above, implied by the length l_{deemb} in Fig. 12(a).

It is assumed that the post in Fig. 12(a) has a square footprint of length t , a height h (which is smaller than the waveguide height b), and an offset from the center position o_c . The basic dependencies of the coupling coefficient K from these parameters are shown in Figs. 13(a)–13(c). In Fig. 13(a), the footprint of the post is varied. Obviously, the position of the TZ generated by the

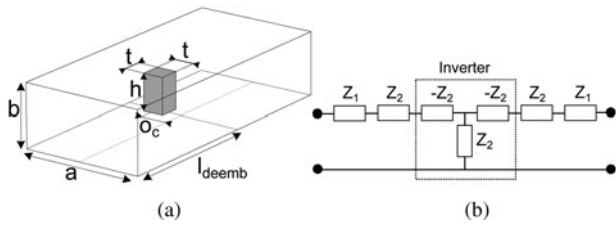


Fig. 12. (a) Partial height post with height h , side-length t , and offset from the center position o_c in a waveguide channel, (b) discrete equivalent circuit from [5].

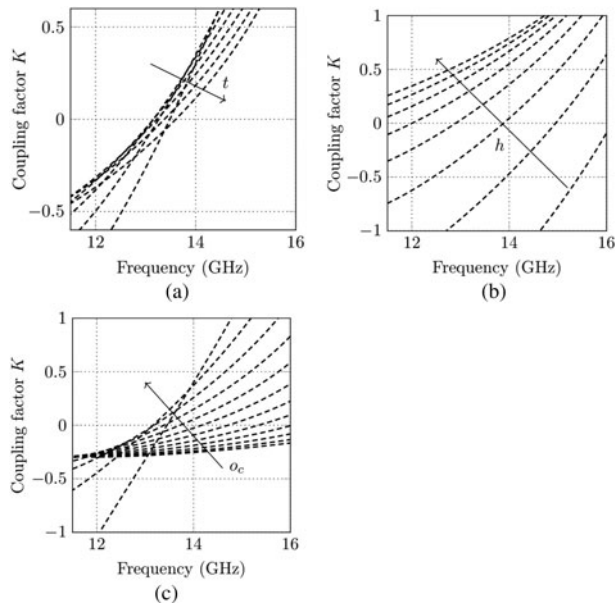


Fig. 13. Parameter study of the post coupling structure for the variation of (a) the footprint ($1\text{ mm} \leq t \leq 4\text{ mm}$ with fixed parameters $h=4.61\text{ mm}$ and $o_c=5.13\text{ mm}$), (b) the height ($3.25\text{ mm} \leq h \leq 6.75\text{ mm}$ with fixed parameters $t=2.55\text{ mm}$ and $o_c=5.13\text{ mm}$) and (c) the offset from the center position ($1\text{ mm} \leq o_c \leq 6\text{ mm}$ with fixed parameters $t=2.55\text{ mm}$ and $h=4.61\text{ mm}$).

post (indicated by the zero-crossing) is only minor affected whereas the coupling factor can be adapted by the parameter t . The position of the TZs might be adapted by the height h as well as the offset of the post o_c , as shown in Figs. 13(b) and 13(c). Depending on both parameters, TZs above and below the passband can be realized.

For the realization of the coupling scheme in Fig. 11(a), a partial height post is inserted in the source port and a second one in the load port, replacing the former inductive irises. The design of the posts dimensions might follow the coupling matrix synthesis technique as proposed in [5, 24]. However, it is also possible to use the following procedure to find the physical dimensions of the posts with standard coupling matrix and optimization techniques:

- (1) Based on the dependencies found in Fig. 13, the TZ generated from the post is shifted relatively far away from the passband by e.g. increasing the post height.
- (2) As subsequently no TZ is generated from the post in the near vicinity of the passband, standard coupling matrix extraction techniques can be used for initial filter tuning, e.g. [25].
- (3) In the next step, the TZ is shifted step-by-step close to the passband at the desired position, where de-tuning effects

Table 2. Dimensions of the posts in the source/load port.

	Post in S-1 coupling	Post in 4-L coupling
Offset o_c	5.12 mm	5.29 mm
Height h	4.61 mm	4.61 mm
Footprint t	2.55 mm	2.69 mm

Table 3. Coupling matrix M_1 to fit the S-parameters in Fig. 14

	S	1	2	3	4	L
S	0.0	0.899	0.0001	0.0	-0.018	0.0
1	0.899	0.155	0.698	0.0	-0.144	0.0
2	0.0001	0.698	0.191	0.606	0.030	0.0
3	0.0	0.0	0.606	0.019	0.835	0.0
4	-0.018	-0.144	0.030	0.835	-0.038	1.123
L	0.0	0.0	0.0	0.0	1.123	0.0

might be compensated by optimization techniques in a full-wave simulator, e.g. the Trust Region Framework in CST Microwave Studio.

The standard design (without SL coupling) in Fig. 1 reveals three TZs, two of which above and one below the passband (compare also the measurement results in Fig. 3). Two TZs are now added below the passband by using the partial height posts. The post in the source port is designed to realize a TZ at 13.05 GHz, while the post in the load port reveals a TZ at 13.48 GHz. Dimensions as shown in Table 2 were found for the posts.

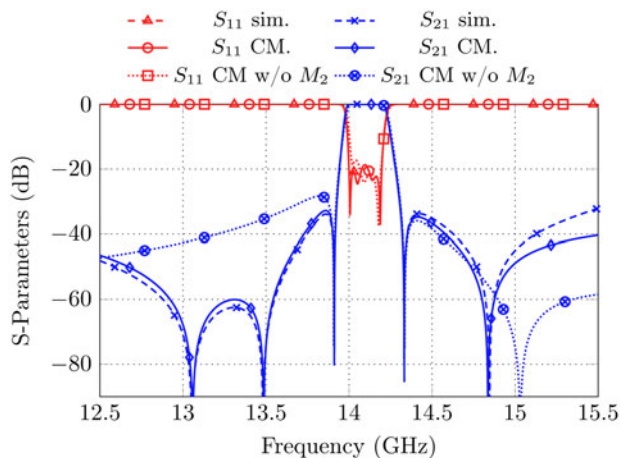
A coupling matrix description is possible if the frequency-dependent couplings are considered in e.g. the optimization procedure. The starting point is the well-known impedance matrix description of a coupled resonator filter given by [1]

$$[Z] = [jM_1 + sM_2 + R] \tag{7}$$

with M_1 is the classical $(n+2) \times (n+2)$ coupling matrix and s is the complex lowpass frequency variable. M_2 is an identity matrix which accounts for the frequency dependence of the resonators and is therefore zero at positions (1, 1) and $(n+2, n+2)$. The matrix R accounts for the resistive source and load terminations and has therefore entries only at position (1, 1) and $(n+2, n+2)$. The frequency dependence of the couplings m_{S1} , m_{S2} , m_{S4} as well as m_{4L} can now be accommodated in matrix M_2 . For the generation of the impedance matrix (7), the coupling matrix in Table 1 is used as a starting point for the optimization and only the frequency-dependent entries in M_2 are varied. To achieve a sufficient good fit between the simulation and the coupling matrix, all entries in M_1 and M_2 are optimized in a second step. The results are shown in Tables 3 and 4. Note, that the appearance of the frequency-independent coupling matrix in Table 3 is very similar to the one of the basic set-up as shown in Table 1. Figure 14 compares the simulated S-parameters of the filter set-up in Fig. 11 with the S-parameters from the coupling matrices from Tables 3 and 4. A very good agreement over nearly the whole frequency region is achieved. Furthermore, the dotted lines illustrate the frequency

Table 4. Coupling matrix M_2 to fit the S-parameters in Fig. 14

	S	1	2	3	4	L
S	0.0	0.071	0.016	0.0	-0.003	0.0
1	0.071	1	0.0	0.0	0.0	0.0
2	0.016	0.0	1	0.0	0.0	0.0
3	0.0	0.0	0.0	1	0.0	0.0
4	-0.003	0.0	0.0	0.0	1	0.215
L	0.0	0.0	0.0	0.0	0.215	0.0

**Fig. 14.** Simulated S-parameters in comparison to the S-parameters generated by the coupling matrices.

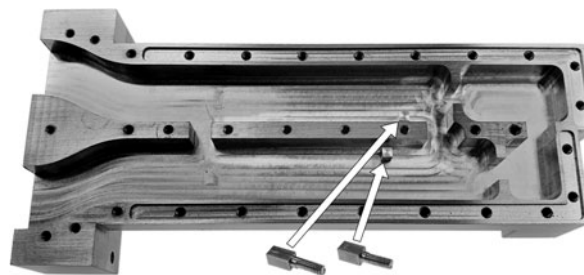
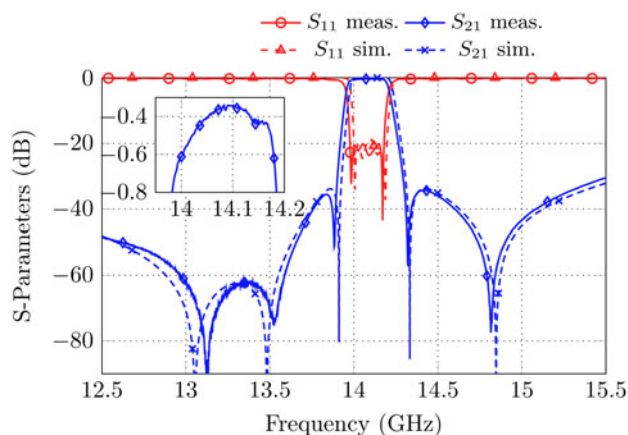
response of only the frequency-independent coupling matrix M_1 . Three TZs are present, while the outer TZ is shifted to higher frequencies. However, if the frequency-dependent coupling matrix is taken into account as well, five TZs arise. The three TZs below the passband are realized by the partial height posts and by the cross-coupling of cavities one and four.

As a proof of concept, the filter was manufactured in aluminum (AlMg3), as shown in Fig. 15. The direct source to load cross-coupling can be closed by a small brick and is therefore only used in the second measurement. The posts are very close to the side wall of the waveguide channel. It is therefore not possible to manufacture them in one piece with the waveguide filter due to milling issues. Hence, the posts are manufactured separately with a thread on the lower side. Holes are foreseen at the post position in the waveguide filter and after manufacturing all posts can be screwed at the desired positions.

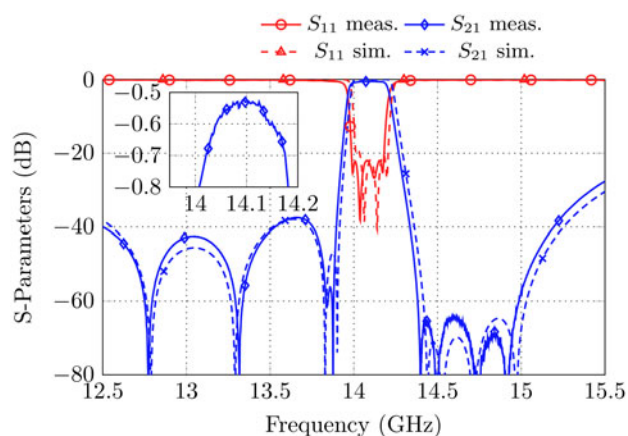
The measured S-parameters in comparison to the simulation are shown in Fig. 16. The insertion loss in the passband is on average approximately 0.5 dB, which corresponds to a quality factor of $Q_u \approx 3200$.

Measurement set-up with additional source to load cross-coupling

The filter in Fig. 15 is able to realize additional TZs by using the direct source to load cross-coupling. The aperture was positioned at $s_0 = 44$ mm and $d_{SL} = 5.45$ mm. The position was found by parameter sweeps as an analytical calculation of the position to reproduce a certain TZ pattern is not possible until now. The

**Fig. 15.** Manufactured fourth-order waveguide filter with frequency-dependent couplings in the source and load port for the realization of the coupling scheme in Fig. 11. The direct source to load coupling slot is closed by a small brick for the measurement results in section “Filter set-up without source to load cross-coupling” and only used for the measurements in section “Measurement set-up with additional source to load cross-coupling”.**Fig. 16.** Measurement results in comparison to the simulation for the filter set-up with frequency-dependent couplings in the source and load port.

S-parameter response is shown in Fig. 17, revealing very good agreement between measurement and simulation. A small frequency shift might be observed which occurs due to the chosen tuning state. Again, four TZs above the passband between 14.4 and 15 GHz very similar to the former measurements can be observed. In this frequency region, an attenuation of better than

**Fig. 17.** Measurement results in comparison to the simulation for the filter set-up with frequency-dependent couplings in the source and load port with additional direct source to load cross-coupling.

60 dB can be reached. The TZ pattern below the passband differs from the one in Fig. 10. Two TZs very close to the passband realize a steep slope and two further TZs at 13.4 GHz as well as at 12.75 GHz can be observed. The attenuation behavior below the passband is better than 38 dB over the whole frequency region. The inset of the plot shows a close-up of the measured insertion-loss. Compared to the former measurements in Fig. 16, higher losses arise. A Q -factor of approximately $Q_u \approx 2600$ can be calculated. The reason for the lower Q -factor compared to the first measurement in Section “Filter set-up without source to load cross-coupling” might be that the screws for the cover were not pulled tight enough or an increasing oxide film reduces the electrical conductivity at the transitions between cover/bottom and the flanges.

Conclusion

In this paper, a fourth-order Ku-band filter for the realization of multiple TZs is investigated. Based on the initial design, which is able to realize seven TZs in the useful Ku-band frequency range, three additional set-ups are investigated in this paper. The first set-up shows the versatility of the proposed configuration as by small changes a phase-equalized filter can be implemented. This filter is able to realize in total up to six TZs, while two of which are complex. Eight real frequency axis TZs can be realized by a similar filter with double slotted source to load cross-coupling. Finally, frequency-dependent couplings are added to the basic filter set-up. As a result, five TZs are obtained for the set-up without an SL coupling while again eight TZs are realized by the set-up with SL coupling. Three simulation results were proven by measurements, which show very good agreement with the simulation over nearly the whole frequency band. Furthermore, two coupling matrices to model the filter with six and seven TZs are derived and a frequency-dependent coupling matrix to model a five TZ filter set-up is proposed.

Acknowledgements. The authors would like to thank M. Mrozowski and A. Lamecki for valuable discussion about frequency-dependent coupling apertures.

References

1. Cameron RJ, Kudsia CM and Mansour RR (2007) *Microwave Filters for Communication Systems*. Hoboken, NJ, USA: Wiley.
2. Montejo-Garai JR and Rebillar JM (2001) Synthesis and design of n -order filters with n -transmission zeros by means of source-load direct coupling. *Microwave and Optical Technology Letters*, **29**, 248–252.
3. Bastioli S (2011) Nonresonating mode waveguide filters. *IEEE Microwave Magazine*, **12**, 77–86.
4. Amari S and Rosenberg U (2005) Characteristics of cross (bypass) coupling through higher/lower order mode and their applications in elliptic filter design. *IEEE Transactions on Microwave Theory and Techniques*, **53**, 3135–3141.
5. Szydlowski L, Lamecki A and Mrozowski M (2012) Coupled-resonator waveguide filter in quadruplet topology with frequency-dependent coupling – a design based on coupling matrix. *IEEE Microwave and Wireless Components Letters*, **22**, 553–555.
6. Szydlowski L and Mrozowski M (2014) A self-equalized waveguide filter with frequency-dependent (resonant) couplings. *IEEE Microwave and Wireless Components Letters*, **24**, 769–771.
7. Politi M and Fossati A (2010) Direct coupled waveguide filters with generalized Chebyshev response by resonating coupling structures. *40th European Microwave Conference*. Paris, France: IEEE.
8. Rosenberg U, Amari S and Seyfert F (2010) Pseudo-elliptic direct-coupled resonator filters based on transmission-zero-generating irises. *40th European Microwave Conference*. Paris, France: IEEE.
9. Miek D, Reinhardt A, Daschner F and Höft M (2018) Improved fully canonical W-band waveguide filter. *Proceedings of the International Microwave Symposium (IMS)*. Philadelphia, PA, USA: IEEE, pp. 1245–1248.
10. Miek D, Morán-López A, Ruiz-Cruz JA and Höft M (2018) Improved fully canonical phase equalized W-band waveguide filter with dispersive coupling inverter. *48th European Microwave Conference (EuMC)*. Madrid, Spain: IEEE, pp. 166–169.
11. Miek D and Höft M (2019) Realization of folded W-band waveguide filters with additional asymmetric resonant transmission zeros. *12th German Microwave Conference (GeMiC)*. Stuttgart, Germany: IEEE.
12. Mokhtari M, Bornemann J, Rambabu K and Amari S (2006) Coupling-matrix design of dual and triple passband filters. *IEEE Transactions on Microwave Theory and Techniques*, **54**, 3940–3946.
13. Miek D, Morán-López A, Ruiz-Cruz JA and Höft M (2019) Ku-band waveguide filter with multiple transmission zeros by resonant source to load and bypass cross-coupling. *49th European Microwave Conference (EuMC)*. Paris, France: IEEE.
14. Cameron RJ (2003) Advanced coupling matrix synthesis techniques for microwave filters. *IEEE Transactions on Microwave Theory and Techniques*, **51**, 1–10.
15. Hong JS and Lancaster MJ (2001) *Microstrip Filters for RF/Microwave Applications*. Hoboken, NJ, USA: John Wiley & Sons Inc.
16. Lampérez AG, Sarkar TK and Palma MS (2002) Filter model generation from scattering parameters using the Cauchy method. *32nd European Microwave Conference*.
17. Miek D and Höft M (2019) Fully reconfigurable hexagonal-shaped comb-line filterplatform for prototyping and education purposes. *International Journal of Microwave and Wireless Technologies*, **12**, 13–20.
18. Rosenberg U (1995) New ‘planar’ waveguide cavity elliptic function filters. *25th European Microwave Conference*. Bologna, Italy: IEEE.
19. Lampérez AG, Sarkar TK and Palma MS (2004) Generation of accurate rational models of lossy systems using the Cauchy method. *IEEE Microwave and Wireless Components Letters*, **14**, 490–492.
20. Amari S, Rosenberg U and Bornemann J (2002) Adaptive synthesis and design of resonator filters with source/load-multiresonator coupling. *IEEE Transactions on Microwave Theory and Techniques*, **50**, 1969–1978.
21. Szydlowski L, Lamecki A and Mrozowski M (2013) A novel coupling matrix synthesis technique for generalized Chebyshev filters with resonant source-load connection. *IEEE Transactions on Microwave Theory and Techniques*, **61**, 3568–3577.
22. Rosenberg U and Amari S (2007) A novel band-reject element for pseudoelliptic bandstop filters. *IEEE Transactions on Microwave Theory and Techniques*, **55**, 742–746.
23. Szydlowski L, Lamecki A and Mrozowski M (2012) Coupled-resonator filters with frequency-dependent couplings: coupling matrix synthesis. *IEEE Microwave and Wireless Components Letters*, **22**, 312–314.
24. Szydlowski L, Leszczynska N and Mrozowski M (2014) Dimensional synthesis of coupled-resonator pseudoelliptic microwave bandpass filters with constant and dispersive couplings. *IEEE Transactions on Microwave Theory and Techniques*, **62**, 1634–1646.
25. Macchiarella G and Traina D (2006) A formulation of the cauchy method suitable for the synthesis of lossless circuit model of microwave filter from lossy measurements. *IEEE Microwave and Wireless Components Letters*, **16**, 243–245.



Daniel Miek received the B.Sc. and M.Sc degrees in electrical engineering and information technology from the University of Kiel, Kiel, Germany in 2015 and 2017, respectively, where he is currently pursuing the Dr.-Ing. degree as a member of the Chair of Microwave Engineering with the Institute of Electrical Engineering and Information Technology. His current research interest includes the design, realization, and optimization of microwave filters as well as parameter extraction and computer-aided tuning.



Patrick Boe received the B.Sc. and M.Sc. degrees in electrical engineering, information technology and business management from Kiel University, Kiel, Germany, in 2017 and 2019, respectively. Currently he is pursuing the Dr.-Ing. degree as a member of the Chair of Microwave Engineering with the Institute of Electrical Engineering and Information Technology. His current research interest

includes the design, realization, and optimization of dielectric resonator filters as well as dielectric multi-mode filters.



Fynn Kamrath received the B.Sc. and M.Sc. degrees in electrical engineering and information technology from Kiel University, Kiel, Germany in 2017 and 2019, respectively. Currently he is pursuing the Dr.-Ing. degree as a member of the Chair of Microwave Engineering with the Institute of Electrical Engineering and Information Technology. His current research interests include the design,

realization, and optimization of center frequency and bandwidth tunable microwave filters in the Ka-Band.



Michael Höft was born in Lübeck, Germany, in 1972. He received the Dipl.-Ing. degree in electrical engineering and Dr.-Ing. degree from the Hamburg University of Technology, Hamburg, Germany, in 1997 and 2002, respectively. From 2002 to 2013, he joined the Communications Laboratory, European Technology Center, Panasonic Industrial Devices Europe GmbH, Lüneburg, Germany.

He was a Research Engineer and then Team Leader, where he had been engaged in research and development of microwave circuitry and components, particularly filters for cellular radio communications. From 2010 to 2013, he had also been a Group Leader for research and development of sensor and network devices. Since October 2013 he is a Full Professor at the Kiel University, Kiel, Germany in the Faculty of Engineering, where he is the Head of the Microwave Group of the Institute of Electrical and Information Engineering. His research interests include active and passive microwave components, (sub-) millimeter-wave quasi-optical techniques, and circuitry, microwave, and field measurement techniques, microwave filters, microwave sensors, as well as magnetic field sensors. Dr. Höft is a member of the European Microwave Association (EuMA), the association of German Engineers (VDI), a member of the German Institute of Electrical Engineers (VDE), and a senior member of IEEE.